Formation and Characterization of Crystalline Molecular Arrays of Gas Molecules in a 1-Dimensional Ultramicropore of a Porous Copper Coordination Polymer

Ryo Kitaura,[†,#] Ryotaro Matsuda,[†] Yoshiki Kubota,[‡] Susumu Kitagawa,*[,†] Masaki Takata,[§] Tatsuo C. Kobayashi,[⊥] and Megumi Suzuki[⊥]

Department of Synthetic Chemistry and Biological Chemistry, Kyoto University, Katsura, Nishikyo-ku, Kyoto 615-8510, Japan, Department of Natural Science, Osaka Women's University, Sakai, Osaka 590-0035, Japan, JASRI-the SPring-8, Koto 1-1, Hyogo 679-5198, Japan, and Department of Physics Faculty of Science, Okayama University Tsushima-naka, Okayama 700-8530, Japan

Received: August 8, 2005; In Final Form: October 9, 2005

Molecules and atoms confined in a nanospace may have properties distinctly different from those of the bulk fluid, owing to the formation of a specific molecular array characteristic of nanospace. In situ synchrotron powder X-ray diffraction measurements have been used to observe confined guest molecules such as N_2, O_2, Ar, and CH_4 in the well-regulated ultramicropore of a copper coordination polymer, **1** ($[Cu_2(pzdc)_2pyz]$: pzdc = 2,3-pyrazinedicarboxylate and pyz = pyrazine). The obtained crystal structures indicate that guest molecules are confined in a linear fashion to form crystalline-like regular ordered arrays, in contrast to the situation in the gas and liquid state, even at temperatures above the boiling point, and the ordered arrays are characteristic of the kind of gas molecule and the geometrical and potential properties of the ultramicropore of **1**.

Introduction

Molecules adsorbed in microporous materials tend to form a specific molecular assembly subjected to their restricted porous geometry and the adsorption enhancement effect of multiple attractive interactions exerted from the confronting and neighboring pore walls; this is characteristic of the nanometer-sized space of a micropore (pore size < 2 nm). This adsorption enhancement effect has been widely studied not only for its industrial application with gas storage materials and heterogeneous catalysts, but also for the unique properties of confined molecules that are distinctly different from those of the bulk fluid. For example, it has been reported that molecules confined in a micropore show an abnormal freezing and melting behavior, high Second-Harmonic Generation (SHG) activity, and specific magnetic properties.[1−5] Therefore, confinement of molecules in a nanometer-sized space would lead not only to finding novel phenomena, but also to providing novel magnetic, electric, and photophysical materials, which we call a "nanospace laboratory".[6] To develop a nanospace laboratory, a better understanding of the adsorption phenomena and detailed structural information of confined guest molecules is indispensable. Although a great deal of useful and interesting information is available about adsorption and confinement phenomena of guest molecules in microporous materials—including molecular simulations such as molecular dynamics and Monte Carlo simulations, thermodynamic studies such as sorption isotherms and heat measurements, nuclear magnetic resonance measurements, and in situ X-ray small-angle scattering measurements—details of the ordered state of confined molecules remain elusive.[7−14]

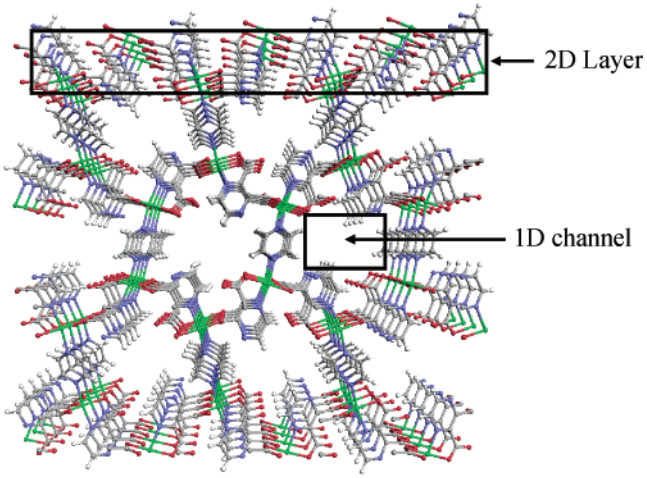

Figure 1. Crystal structure of $\{[Cu_2(pzdc)_2pyz]\cdot 2H_2O\}_n$ (**1** ⊃ H_2O) along the *a* axis. Green, blue, white, gray, and red balls and sticks represent the Cu, nitrogen, hydrogen, carbon, and oxygen atoms, respectively. Solvated water molecules are omitted for clarity.

Consequently, we have tried to perform a direct observation of the guest molecules confined in microporous materials using in situ synchrotron X-ray diffraction.

Recently, many crystalline porous coordination polymers that are constructed from metal ions and bridging ligands have been synthesized and studied for their adsorption performance with various gas molecules.[9,15−25] Porous coordination polymers have advantages over the conventional microporous materials such as activated carbon and zeolites: (1) well-regulated and designable nanochannels, and (2) a variety of nanochannels ranging from one- to three-dimensional types.[6,26−30] These features are of key importance in performing direct observation by X-ray crystallography of various molecular assemblies confined in the nanochannel.[31−33] Thus, our strategy for observing regular assemblies of guest molecules is to utilize the well-regulated channels of porous coordination polymers. Figure 1 shows the

* Address correspondence to this author. Phone: 81-75-383-2733. Fax: 81-75-383-2732. E-mail: kitagawa@sbchem.kyoto-u.ac.jp.
[†] Kyoto University.
[#] Current Address: Department of Chemistry, Nagoya University, furocho, Nagoya 464-8602, Japan.
[‡] Osaka Women's University.
[§] JASRI-the SPring-8.
[⊥] Okayama University.

10.1021/jp054411j CCC: $30.25 © 2005 American Chemical Society
Published on Web 11/16/2005

TABLE 1: Chemical Composition and Crystallographic Details of the Guest Molecule Adsorbed 1

	N_2	O_2	Ar	CH_4
formula	$C_{16}H_8Cu_2N_{10}O_8$	$C_{16}H_8Cu_2N_6O_{12}$	$C_{16}H_8Cu_2N_6O_8Ar_2$	$C_{18}H_{16}Cu_2N_6O_8$
fw	595.39	603.36	619.26	571.45
cryst system	monoclinic	monoclinic	monoclinic	monoclinic
space group	$P2_1/c$ (no. 14)	$P2_1/c$ (no. 14)	$P2_1/c$ (no. 14)	$P2_1/c$ (no. 14)
a, Å	4.69653(10)	4.68759(4)	4.67346(9)	4.6691(5)
b, Å	20.54323 (22)	20.4373(2)	20.25969(19)	20.0545(3)
c, Å	11.03197(16)	10.9484(1)	11.15928(21)	11.4524(1)
β, deg	97.4518(20)	96.9480(6)	97.2824 (19)	98.4005(8)
V, Å^3	1055.39(5)	1041.17(3)	1048.069(5)	1060.85(14)
diffractometer	Debye−Scherrer	Debye−Scherrer	Debye−Scherrer	Debye−Scherrer
λ, Å	0.80047	0.80092	0.80093	0.80138
R_I[a]	0.038	0.039	0.048	0.025
R_{wp}[b]	0.018	0.041	0.015	0.037
R_F[c]	0.022	0.015	0.011	0.013

[a] $R_I = \sum||I_O| - |I_C||/\sum I_O$. [b] $R_{wp} = [\sum w\{y_O - y_C\}^2/\sum w y_O^2]^{1/2}$. [c] R factor based on MEM analysis.

structure of a three-dimensional (3D) porous copper coordination polymer, **1** ($[Cu_2(pzdc)_2pyz]$: pzdc = 2,3-pyrazinedicarboxylate and pyz = pyrazine), determined by a single-crystal diffraction study.[34] Two-dimensional sheets constructed by Cu ions and pzdc ligands are linked by pillar ligands (pyz) to form a 3D pillared-layer structure. This framework possesses a small one-dimensional (1D) channel, which is categorized in the ultramicropore range (dimensions of ca. 4.0 × 6.0 Å^2). Herein we report a detailed sorption study and direct observation of simple gas molecules such as O_2, N_2, Ar, and CH_4, adsorbed in the 1D ultramicropore of **1** by synchrotron powder X-ray diffraction measurements and maximum entropy method (MEM)/Rietveld analyses. Hereafter, guest adsorbed **1** is denoted as **1** ⊃ G (G = H_2O, O_2, N_2, Ar, and CH_4). Each small molecule possesses a different size, shape, dipole moment, quadrupole moment, and magnetic moment (for example only the O_2 molecule has a magnetic moment, $S = 1$), which operate on the interaction force between adsorbed molecules and/or the pore walls. This is the first systematic observation of physisorbed gas molecules in a porous solid, which will contribute to a better understanding of physisorption phenomena based on intermolecular interactions, and will lead to the development of the rational design of high-performance gas storage material, and further, to establishment of the nanospace laboratory.

Experimental Section

1. Synthesis of $\{[Cu_2(pzdc)_2pyz]\cdot 2H_2O\}_n$ (1 ⊃ H_2O). A water solution (2.5 mL) of Na_2pzdc (10 mM) was carefully layered on the top of a water solution (2.5 mL) of $Cu(ClO_4)_2$-$6H_2O$ (10 mM) and pyz (200 mM) in a quarts glass tube. Blue needle crystals began to form in a week. The obtained needle crystals were collected by filtration, washed with water, and dried under reduced pressure for 5 h at room temperature. Yield: 0.26 g (0.45 mmol, 45%). Anal. Calcd for $C_{16}H_{12}$-$Cu_2N_6O_{10}$: C, 33.40; H, 2.10; N, 14.61. Found: C, 32.78; H, 1.57; N, 14.34. IR (KBr disk) (cm^{-1}): 3436 br, 3092 w, 1655 s, 1586 s, 1468 m, 1399 s, 1346 m, 1235 w, 1202 w 1183 w, 1157 w, 1129 s, 1073 m, 903 m, 855 m, 841 w, 758 w, 615 w, 558 w, 490 m, 449 w.

2. Physical Measurements. Elemental analyses were taken on a Yanaco C,H,N Corder MT-5. IR spectra were recorded on a Hitachi I-5040FT-IR spectrometer with samples prepared as KBr pellets.

3. Gas Adsorption Measurements. The adsorption isotherms of Ar, CH_4, N_2, and O_2 at 77 K and of CO_2 at 195, 273, 283, 293, 300, and 310 K were measured with BELSORP-18 (BEL Inc.) automatic volumetric adsorption equipment. A known weight (200−300 mg) of the as-synthesized **1** (**1** ⊃ H_2O) was placed in the quarts tube, then, prior to measurements, the sample was outgassed under vacuum ($P < 10^{-5}$kPa) at 373 K for 5 h to remove the solvated water molecules. The adsorbate was dosed into the sample tube, then the change of pressure was monitored and the amount of adsorption was determined by the decrease of pressure at the equilibrium state.

4. X-ray Structure Determination. Crystal structure determination was carried out from powder diffraction data. X-ray powder diffraction patterns with high resolution and good counting statistics were collected by synchrotron radiation X-ray powder diffraction experiments with an imaging plate (IP) as a detector at the SPring-8 BL02B2. The powder crystal was sealed in the glass capillary (0.4 mm inside diameter). To obtain in situ powder X-ray diffraction patterns, the gas-handling system, which possesses valves and pressure gauges to dose and remove guest molecules, was connected to the goniometer head by a stainless steel line. Cell parameters were determined by the indexing program DICVOL91.[35] The Le Bail structureless profile fitting algorithm affords refined cell parameters, peak shift parameters, and profile parameters. The peak shape was modeled by a Split-Pearson VII function. The structural parameters were refined by Rietveld analysis with soft constraints about bond angles and bond distances throughout the refinement. Hydrogen atoms were located at the ideal position and their parameters were not refined. After the Rietveld structure refinement, the electron density distribution was obtained by the Maximum Entropy Method (MEM). Crystal data and details of the structure determinations are summarized in Table 1.

Results and Discussion

1. Gas Adsorption Properties. Figure 2a shows adsorption isotherms of Ar, CH_4, N_2, and O_2 at 77 K and CO_2 at 195 K on **1**. The isotherms display a steep rise at the low relative pressure region followed by a plateau region. All of the adsorption isotherms can be categorized as isotherms of Type I, indicative of a typical physisorption process of the microporous compound. The low onset pressure and sharp rise of the isotherm indicate that an extremely uniform and deep potential well forms in the ultramicropore of **1**. The deep potential well can also be confirmed by the isosteric heat of adsorption, which was calculated according to the following equation by using CO_2 adsorption isotherms measured at 273, 283, 293, 300, and 310 K (Figure 2c):

$$q_{st} = -R\left(\frac{\partial \ln P}{\partial (1/T)}\right)_N \quad (1)$$

where q_{st}, R, P, and N represent the isosteric heat of adsorption,

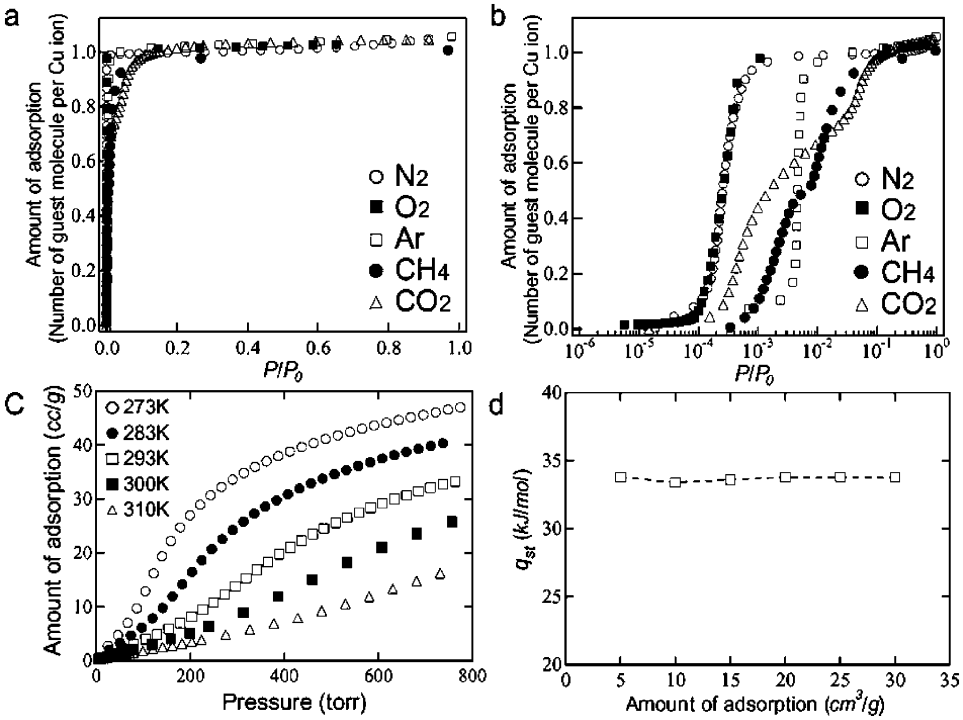

Figure 2. Adsorption isotherms of **1**. (a) Adsorption isotherms for N_2, O_2, Ar, and CH_4 at 77 K and CO_2 at 195 K in the relative pressure range from 10^{-5} to 0.95. (b) Adsorption isotherms for N_2, O_2, Ar, and CH_4 at 77 K and CO_2 at 195 K plotted against the common logarithm of the relative pressure. (c) Adsorption isotherms for CO_2 of **1** at 273, 283, 293, 300, and 310 K. (d) Calculated isosteric heat of adsorption of CO_2 on **1** plotted against the amount of adsorption.

gas constant, pressure, and the amount of adsorption of CO_2, respectively. The obtained value for q_{st} was 34.3 kJ/mol (at the amount of adsorption of 5.0 cm^3/g), which is much greater than the values for physisorption on mesoporous silicas (ca. 20.0 kJ/mol).[36] Figure 2b shows adsorption isotherms plotted against the common logarithm of P/P_0 in order to differentiate the profile in the low-pressure regions. The molecular size and shape of O_2 and N_2 are similar; therefore, the adsorption isotherms of O_2 and N_2 are almost identical, showing a sudden rise at a relative pressure (P/P_0) of about 10^{-4} and complete coverage above about 10^{-3}. On the other hand, adsorption isotherms of CO_2, CH_4, and Ar show a higher onset pressure than those of O_2 and N_2, which is associated with the entrance blocking effect.[37] Molecular dimensions of CO_2, CH_4, and Ar (3.189, 3.829, and 3.405 Å, respectively) are greater than those of N_2 and O_2 (2.991 and 2.930 Å, respectively) and close to the pore size of **1**.[38] Therefore, a higher relative pressure is required to cross the potential barriers and to induce a distortion of the channel structure. A step in the adsorption isotherms of CO_2 and CH_4 at 0.7 CO_2/Cu and 0.5 CH_4/Cu is attributed to the adsorbate structural change from a metastable phase with a low packing density to a stable phase with a saturated packing density.

Table 2 shows the density of the adsorbed phase, which is calculated according to the following equation:

$$d = \frac{A}{d_{ads}} \tag{2}$$

where d, A, and d_{ads} represent the adsorbate phase density, the amount of adsorption (g/g), and the pore volume of **1** (0.0938 cm^3/g), respectively. The pore volume was defined as solvent (2.4 Å diameter sphere) accessible volume, and this was calculated based on the single-crystal structure of **1** ⊃ H_2O. Interestingly, even under lower pressure than the saturated vapor pressure, the densities of the adsorbed phases of N_2 and O_2 are much greater than those of the corresponding bulk liquid phases, and that of CO_2 is greater than that of the bulk solid phase. On the other hand, the density of the adsorbed phases of CH_4 and Ar is less than those of each bulk liquid state. This indicates that the adsorbed phases are significantly different from the corresponding bulk state and, therefore, are considered to be a new state characteristic of molecules confined in the ultramicropore of **1**.

TABLE 2: Density of Confined and Bulk Liquid Phase of N_2, O_2, CO_2, Ar, and CH_4

	N_2	O_2	CO_2	Ar	CH_4
d (g/cm^3)	1.11	1.27	1.74	1.58	0.63
d_{liquid} (g/cm^3)	0.808	1.14	1.56[a]	1.78	0.716

[a] Density of solid CO_2 at 193 K.

TABLE 3: Calculated DR Parameters and Molecular Volumes

	N_2	O_2	Ar	CH_4	CO_2
W_0 (guest/Cu)	1.00	1.02	1.03	1.02	1.04
βE_0 (kJ/mol)	14.1	14.3	13.8	17.2	15.4
V (Å^3)	36.6	30.6	33.5	43.0	45.0

Generally, distinct from chemisorption, in which a guest molecule is bound to specific surface adsorption sites via a chemical bond, physisorption is a nonspecific adsorption without any specific binding sites. Therefore, physisorbed guest molecules tend not to occupy specific surface sites, resulting in formation of a disordered adsorption phase; in this case, the saturated amount of adsorption changes according to the size and volume of the guest molecules. Dubinin−Radushkevich plots are almost linear in the higher relative pressure region, giving the saturated amount of adsorption (W_0) and adsorption characteristic energy (βE_0), which are shown in Table 3 together with the molecular volume of guest molecules (V).[39] Interestingly, despite differences in the molecular volumes of the guest molecules (molecular volume of O_2 is only 68% of that of CO_2,

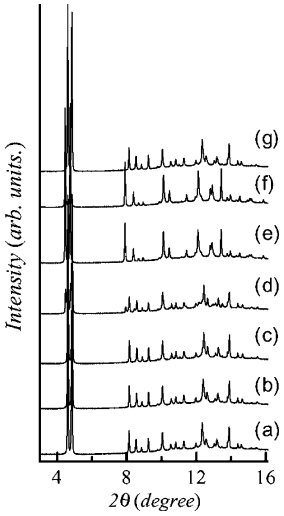

Figure 3. Synchrotron X-ray powder diffraction patterns of anhydrous **1** (after drying at 373 K under reduced pressure) with N_2 of 0.8 atm with cooling from 300 to 90 K and reheating to 300 K. (a−g) XRPD patterns at 300, 200, 150, 130, 110, 90, and 300 K, respectively.

for example), the saturated amount of adsorption of all guest molecules on **1** clearly shows a stoichiometry with just one guest molecule per copper ion, as if there is one specific guest binding site per copper ion. As illustrated in Figure 2d, the isosteric heat of adsorption for CO_2 is unchanged during the adsorption process, indicating that binding sites of **1** are uniform. This, "chemisorption-like physisorption", is attributed to the confinement effect characteristic of the well-regulated ultramicropore of **1**. To elucidate the structure of the adsorbed molecules and binding sites, we performed in situ X-ray powder diffraction (XRPD) measurements.

2. In Situ XRPD Measurements and Structure Determination. Before adsorption of guest molecules, we heated **1** ⊃ H_2O under reduced pressure to remove water molecules from the channel and then dosed it with guest molecules with cooling. This framework is stable without any guest molecules in the channel and achieves permanent porosity, which was confirmed by MEM/Rietveld analysis of anhydrous **1**.[31] Figure 3 shows in situ XRPD patterns of anhydrous **1** with 80 kPa of N_2 over the temperature range 300 to 90 K. Drastic changes of the powder diffraction patterns were observed during cooling, which completely reverted to the original patterns during the reheating process. A similar tendency in X-ray diffraction patterns was observed with O_2, Ar, and CH_4, besides the onset temperatures, where discontinuous change is found in the diffraction patterns. The onset temperatures of the diffraction pattern change are between 150 and 130, 130 and 110, 160 and 140, and 150 and 130 K for O_2, N_2, CH_4, and Ar, respectively. The order of onset temperature, $CH_4 > Ar \approx O_2 > N_2$, is consistent with the boiling point of the guest molecules. Figure 4 shows the temperature dependence of the cell parameters of **1** with N_2 molecules, refined by the LeBail structureless profile fitting algorithm. Elongation of the *b* and *c* axes and shortening of the *a* axis were observed at the onset temperature. As a result of this cell parameter change, a cell volume expansion of about 4% was observed (Figure 4d). These diffraction pattern changes were completely reversible, and no change was observed in the absence of guest molecules over the corresponding temperature range. Therefore, we concluded that this cell volume expansion was triggered by adsorption of N_2 molecules.[9,17,40−42]

The space group of the **1** ⊃ N_2 at 90 K (Figure 3f) was assigned as monoclinic $P2_1/c$ (a = 4.69653(10) Å, b = 20.54323(22) Å, c = 11.03197(16) Å, and β = 97.4518(20)°). The experimental data were analyzed by the MEM/Rietveld method, which was successfully applied to the structure determination of **1** ⊃ O_2.[33] The number of structure factors derived in this analysis was 1309. The reliability (R) factor based on the Bragg intensities R_I and the weighted profile R factor R_{wp} of the preliminary Rietveld fitting were 0.337 and 0.078, respectively. On the basis of this preliminary fitting result, a MEM analysis was performed. An electron density map obtained from the MEM analysis clearly revealed an N_2 molecule feature at the middle of the channel. After revision of the structure model according to this electron density map, Rietveld fitting was dramatically improved, resulting in R_I and R_{wp} becoming 0.038 and 0.018, respectively. The final electron densities, obtained by the MEM whose reliability factor (R_F) was 0.022, clearly reveal the 3D pillared-layer structure consistent with single-crystal data. Figure 5 shows the perspective view of the electron density distribution map along the *a* axis. Peanut-shaped

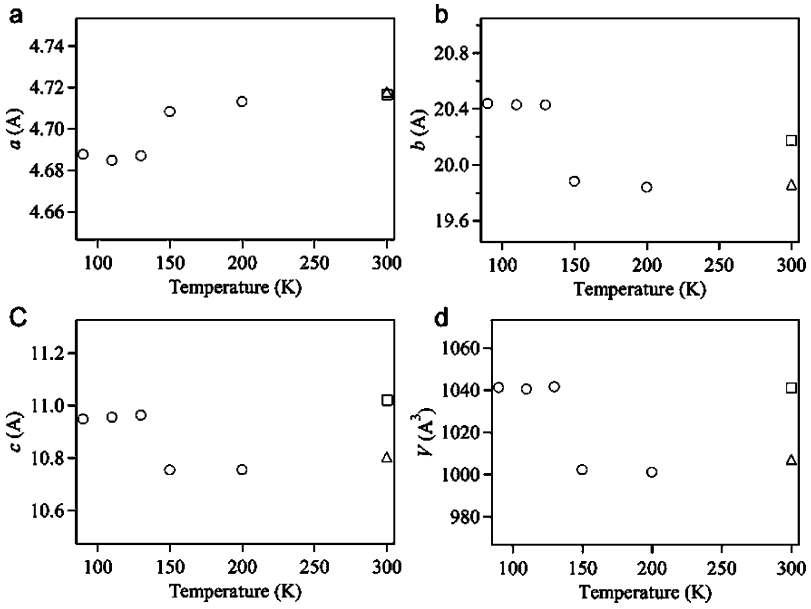

Figure 4. Variation of the lattice parameters and the cell volume of **1** during the cooling process with 0.8 atm of N_2. Squares, triangles, and circles show the data of **1** ⊃ H_2O, anhydrous **1**, and **1** with N_2, respectively

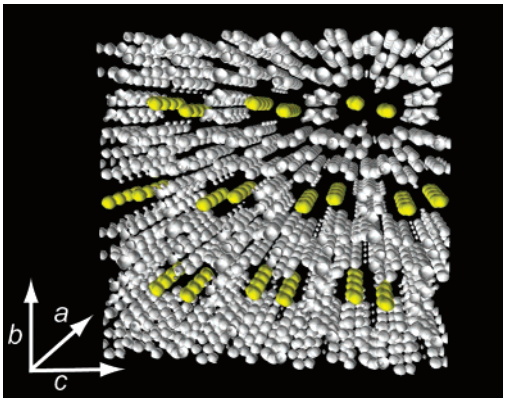

Figure 5. MEM charge density maps of **1** ⊃ N_2 at 90 K as an equi-density contour surface. The equi-contour level is 1.0 eÅ^{-3}.

electron densities are clearly recognized in the interlayer channel, and we conclude that these densities are due to N_2 molecules, and one N_2 molecule was adsorbed per copper atom; this result is consistent with the adsorption isotherm. According to the same procedure shown above, we determined crystal structures of **1** ⊃ Ar, **1** ⊃ CH_4, and **1** ⊃ O_2. Panels a−d of Figure 6 show the results of the final Rietveld fitting of **1** ⊃ N_2, **1** ⊃ Ar, **1** ⊃ CH_4, and **1** ⊃ O_2, respectively. The *R* factors of the final Rietveld fitting and MEM analyses are shown in Table 1.

3. Confinement of Guest Molecules. The overall crystal structure and geometry of N_2 molecules in **1** ⊃ N_2 based on the above analysis are represented in Figure 7a,b. The relatively small value of the isotropic displacement parameter (B = 4.8-(3)) and no disorder of N_2 molecules indicate that the N_2 molecules adsorbed in the ultramicropore were like the solid state rather than the liquid state at 90 K. Furthermore, essentially the same structure of confined N_2 molecules was confirmed even at 110 K according to the same procedure of analysis; this temperature is much higher than the freezing point of N_2 molecules (77 K) at atmospheric pressure. Here, a question

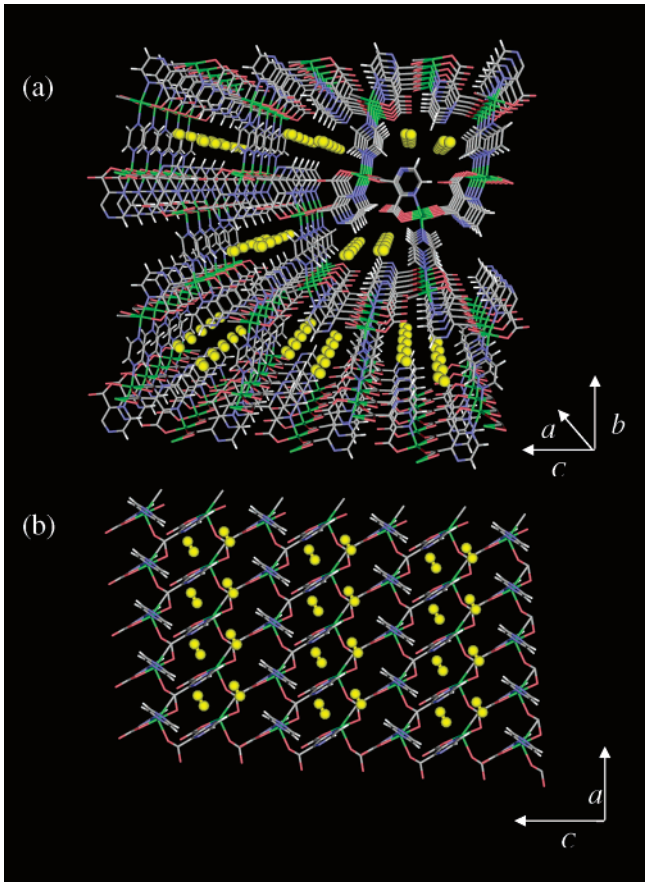

Figure 7. Schematic representation of **1** ⊃ N_2 at 90 K: (a) the perspective view down the *a* axis and (b) the view down the *b* axis. Confined N_2 molecules are denoted as yellow.

arises: Why do N_2 molecules form such a crystalline solid state even at 110 K? This phenomenon is associated with the strong confinement effect of the ultramicropore of **1**, in which two

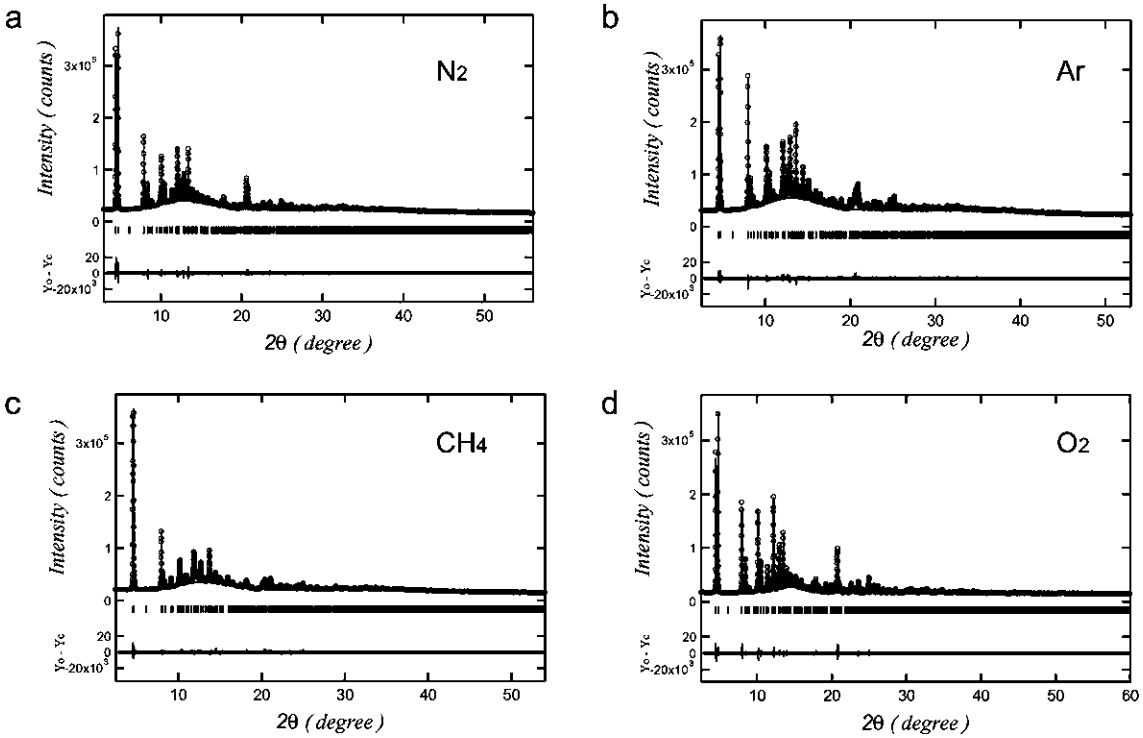

Figure 6. Synchrotron X-ray powder diffraction patterns and the final results of Rietveld fitting of (a) **1** ⊃ N_2 at 90 K, (b) **1** ⊃ Ar at 90 K, (c) **1** ⊃ CH_4 at 110 K, and (d) **1** ⊃ O_2 at 90 K, respectively.

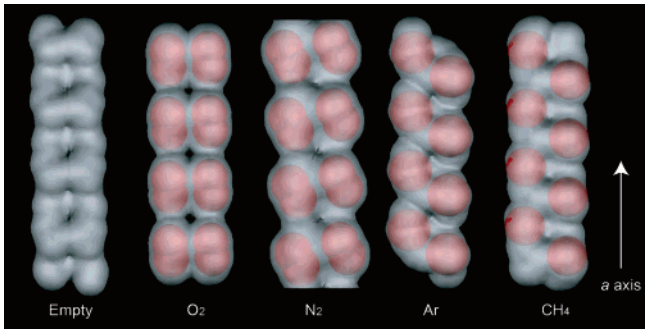

Figure 8. Representation of confined guest molecules drawn by the space filling model (red sphere) and solvent-accessible pore surface, which is defined by the possible surface of a rolling sphere with a diameter 3.0 Å, along the *a* axis.

major factors operate: (1) pore surface geometry such as size and shape and (2) the nature of the molecule−pore surface interaction. The van der Waals interaction that dominates the physisorption process is a nonspecific interaction, which is not very sensitive to pore wall properties. Therefore, factor (1) would be essential for physical adsorption in an ultramicropore; this pore surface can be defined as a possible surface for a sphere of diameter 3.0 Å as it rolls over the surface of the channel in **1**. The pore surface is shown in Figure 8, together with confined guest molecules. The pore surface of empty **1** appears completely different from those of guest adsorbed **1**, and the pore surfaces of **1** ⊃ Ar and **1** ⊃ CH_4 show a different feature from those of **1** ⊃ O_2 and **1** ⊃ N_2. This is attributable to a sort of induced fit resulting from the framework flexibility of **1**.[20,43−47] As is clearly illustrated in Figure 8, concavity and convexity of the channel with a periodicity of about 4.7 Å (namely, the length of the *a* axis) provide pockets that are suitable in shape and size to confine guest molecules. This specific binding pocket should provide a significantly deep potential well along the channel direction. In addition, positively charged Cu ions and negatively charged carboxylate oxygen atoms, which can interact with guest molecules by an orientation force and an induction force, are located at the middle of the pocket (contribution from factor (2)). As a result, guest molecules are strongly confined and stabilized in the pocket, finally forming a crystalline solidlike state. To elucidate this periodic potential well in the ultramicropore of **1**, we calculated the potential curve of **1** ⊃ Ar using the Lennard-Jones (LJ) potential function:

$$U(r) = 4\epsilon\left[\left(\frac{\sigma}{r}\right)^{12} - \left(\frac{\sigma}{r}\right)^{6}\right] \qquad (3)$$

where r, ϵ, and σ represent the distance between the Ar atom and the framework atoms, the well depth of the potential, and the interatomic distance at which the potential equals zero, respectively.[48] The potential parameters (ϵ and σ) of Ar−C, Ar−O, and Ar−H were calculated according to Lorentz−Berthelot mixing rules, and those of Ar−Cu were taken from the literature.[49,50] Figure 9a shows the potential energy plotted against the position of the Ar atom along the *a* axis; the trajectory of the Ar atom is shown by the yellow arrow in the Figure 9b (the coordinates of the Ar atom along the *b* and *c* axes were optimized to minimize potential energy). As is clearly shown in Figure 9 (solid line), there is a significant potential up and down along the channel direction (*a* axis). The position of the potential minimum is 1.07 Å, which virtually agrees with the observed Ar position, shown in Figure 9 by an arrow. There is one potential well per copper ion, so the saturated amount of adsorption was one guest molecule per copper ion, as illustrated

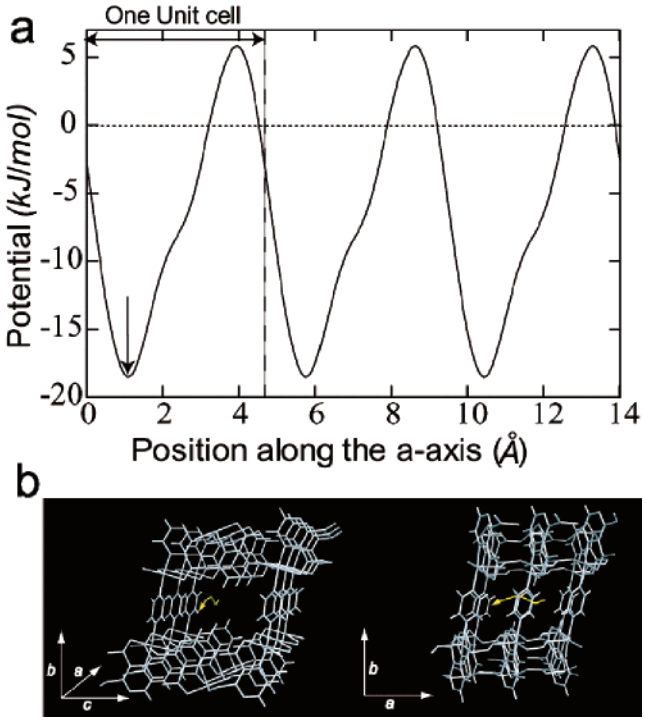

Figure 9. (a) Potential energy plotted against the position of the Ar atom along the *a* axis. (b)Trajectory of the Ar atom in the ultramicropore of **1**.

TABLE 4: Intermolecular Distances of Confined Guest Molecules (d_{obs}) and Lennard-Jones Potential Minimum (d_{min})

	N_2	O_2	Ar	CH_4
d_{obs} (Å)	3.33(2)	3.28(4)	3.60(1)	3.70(1)
d_{min} (Å)	3.67	3.66	3.79	4.18

in Table 3. The minimum of the potential curve is very low (ca. −16 kJ/mol), which clearly shows the deep potential well of the ultramicropore of **1**. It is worth noting that the formation of a crystalline solidlike structure of such simple gas molecules rarely occurs because only a weak and nonspecific intermolecular force (van der Waals force) operates in this system. Contrary to this, aromatic benzene and protic water or methanol molecules easily form ordered arrays due to $\pi-\pi$ interaction and hydrogen bonds.[51] The key to form a low-dimensional crystalline array of small gas molecules is to use the specific pore geometry of the ultramicropore of **1**, which provides molecularly periodic potential up and down (shown in Figures 8 and 9).

Recently, a structural characterization, using X-ray diffraction, of adsorbed Ar and N_2 molecules in the porous coordination polymer, whose pore size is about 12 and 15 Å in diameter, has been reported.[52] On the contrary to **1**, the adsorbed state is not characteristic of confined molecules but like a bulk liquid or solid state because the porous framework used has large pores, which results in lack of ability to form regulated specific low-dimensional molecular arrays as well as activated carbons and mesoporous silicas. To develop "nanospace laboratory", it is crucial to elucidate the structure and to understand the formation mechanism of specific low-dimensional arrays of confined molecules, which are not realized in the bulk state. The results discussed above clearly show that not large pores but the very small pore of **1** is suitable to form a low-dimensional crystalline molecular array.

Table 4 shows the intermolecular distances of confined guest molecules (d_{obs}) together with the minimum of the LJ potential

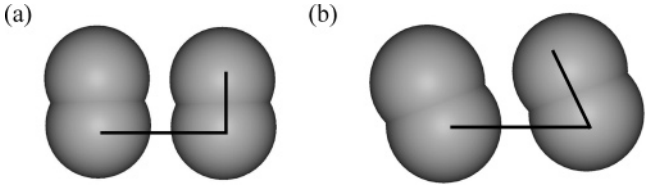

Figure 10. Molecular alignments of (a) O_2 and (b) N_2 van der Waals dimers formed in the ultramicropore of **1**.

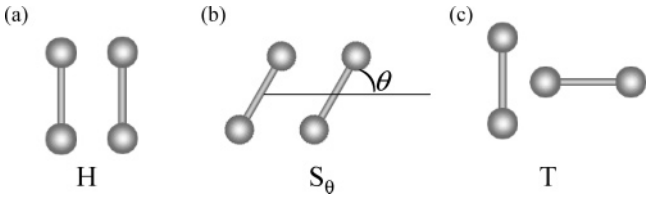

Figure 11. Schematic representation of the dimer alignment of rodlike molecules.

(d_{min}), which was calculated according to the following equation: $d_{min} = 2^{1/6}\sigma$. In all cases, the intermolecular distances of the confined guest molecules are shorter than the minimum of the LJ potential. For example, the intermolecular distance of confined CH_4 molecules is only 90% of that of the LJ potential minimum. At these short intermolecular distances, a repulsive force would act between neighboring guest molecules. Therefore, such a molecular alignment is not stable in the bulk fluid. In contrast, in the ultramicropore of **1**, the strong interactions between the framework and guest molecules mean that energy loss resulting from repulsion between guest molecules can be compensated, thereby achieving the very short intermolecular distances of confined guest molecules as if they were under very high pressure.

4. Formation of van der Waals Dimers. It should be noted that confined N_2 and O_2 in **1** show a dimer feature; the distance between neighboring molecules is much shorter than that to the next neighboring molecules. Figure 10 shows molecular alignments of N_2 and O_2 van der Waals dimers formed in the ultramicropore of **1**. An appreciable difference was observed in the orientation of the confined guest molecules. While O_2 molecules align parallel to the channel of **1**, N_2 molecules inclined against the channel direction to form offset van der Waals dimers. O_2 and N_2 molecules possess quadrupole moments of -1.33×10^{-40} and -4.90×10^{-40} C m^2, respectively.[53] Figure 11 shows a schematic representation of the dimer alignment of a rodlike molecule. Usually, a stable dimer alignment of rodlike molecules having quadrupole moments is T or S_θ type because of an electrostatic interaction resulting from the quadrupole moment (Figure 11b,c). However, in the 1D ultramicropore of **1**, the T type is forbidden because of the restricted space. Therefore, the S_θ type should be the most stable geometry of N_2 dimers in the nanospace of **1**. In contrast, unlike N_2 molecules, the geometry of the O_2 dimer is not the S_θ but the H type. Since the O_2 molecule possesses a triplet spin ground state, the O_2-O_2 dimer has a spin-dependent intermolecular potential.[54,55] This would be one reason the geometry of $(O_2)_2$ is not the S_θ but the H type, despite the energy loss resulting from a repulsion of the quadrupole moments; this alignment maximizes overlap of the antibonding molecular orbitals of the O_2 molecules (π^*) to form antiferromagnetic dimers.[31] This result indicates that the magnetic interaction plays an important role in the geometry of O_2 molecules confined in the ultramicropore of **1**. Studies of van der Waals dimers such as $(O_2)_2$ and $(N_2)_2$ have been widely performed by first-principle calculations and spectroscopic studies, owing to their characteristic properties.[56−58] In general, $(O_2)_2$ and $(N_2)_2$ are stable only under extreme conditions, such as at extremely low temperature in a solid neon matrix, because of their thermal liability. On the other hand, molecules confined in the ultramicropore of **1** easily form van der Waals dimers under mild conditions. This is one of the remarkable examples of the stabilization effect of nanospace, achieving molecular alignments that are not stable under normal conditions.

Conclusions

We have shown that adsorbed gas molecules form specific molecular arrays, which cannot be realized in the bulk fluid. The specific pore geometry provided by the 1D ultramicropore of **1** and intermolecular interactions between guest molecules and/or pore wall play an important role. These specific assemblies were successfully characterized by high resolution in situ synchrotron XRPD measurements and the MEM/Rietveld method. These results are conceptually important not only for the development of gas storage materials with high performance but also for the understanding of micropore filling based on the role of micropore geometry and intermolecular interactions, providing a nanospace laboratory with a potential to discover novel phenomena of molecular assemblies unexplored in the conventional bulk solid and/or gas state.

Acknowledgment. The synchrotron radiation experiments were performed at the SPring-8 with the approval of the Japan Synchrotron Radiation Research Institute (JASRI). We thank Dr. H. Tanaka for the computer program, ENIGMA, for the MEM analysis, and Mr. K. Kato for his experimental help at the SPring-8. This work was supported by a Grant-In-Aid for Science Research in a Priority Area "Chemistry of Coordination Space" (No. 434) from the Ministry of Education, Science, Sports, and Culture, Japan.

References and Notes

(1) Hertzsch, T.; Budde, F.; Weber, E.; Hulliger, J. *Angew. Chem., Int. Ed.* **2002**, *41*, 2281.
(2) Morishige, K.; Kawano, K. *J. Phys. Chem. B* **2000**, *104*, 2894.
(3) Langley, P. J.; Hulliger, J. *Chem. Soc. Rev.* **1999**, *28*, 279.
(4) Atwood, J. L.; Barbour, L. J.; Jerga, A. *Science* **2002**, *296*, 2367.
(5) Terskikh, V. V.; Moudrakovski, I. L.; Ratcliffe, C. I.; Ripmeester, J. A.; Reinhold, C. J.; Anderson, P. A.; Edwards, P. P. *J. Am. Chem. Soc.* **2001**, *123*, 2891.
(6) Kitagawa, S.; Kitaura, R.; Noro, S. *Angew. Chem., Int. Ed.* **2004**, *43*, 2.
(7) Miyahara, M.; Gubbins, K. E. *J. Chem. Phys.* **1997**, *106*, 2865.
(8) Bojan, M. J.; Steele, W. A. *Carbon* **1998**, *36*, 1417.
(9) Fletcher, A. J.; Cussen, E. J.; Prior, T. J.; Rosseinsky, M. J.; Kepert, C. J.; Thomas, K. M. *J. Am. Chem. Soc.* **2001**, *123*, 10001.
(10) Gregg, S. J.; Sing, K. S. W. *Adsorption, Surface Area, and Porosity*; Academic Press: London, UK, 1984.
(11) Nitta, T.; Nozawa, M.; Hishikawa, Y. *J. Chem. Eng. Jpn.* **1993**, *26*, 266.
(12) Iiyama, T.; Nishikawa, K.; Otowa, T.; Kaneko, K. *J. Phys. Chem.* **1995**, *99*, 10075.
(13) Iiyama, T.; Ruike, M.; Kaneko, K. *Chem. Phys. Lett.* **2000**, *331*, 359.
(14) Ratcliffe, C. I.; Soldatov, D. V.; Ripmeester, J. A. *Microporous Mesoporous Mater.* **2004**, *73*, 71.
(15) Eddaoudi, M.; Kim, J.; Rosi, N.; Vodak, D.; Wachter, J.; O'Keeffe, M.; Yaghi, O. M. *Science* **2002**, *295*, 469.
(16) Chui, S. S.-Y.; Lo, S. M.-F.; Charmant, J. P. H.; Orpen, A. G.; Williams, I. D. *Science* **1999**, *283*, 1148.
(17) Cussen, E. J.; Claridge, J. B.; Rosseinsky, M. J.; Kepert, C. J. *J. Am. Chem. Soc.* **2002**, *124*, 9574.
(18) Li, D.; Kaneko, K. *Chem. Phys. Lett.* **2001**, *335*, 50.
(19) Rosi, N. L.; Eckert, J.; Eddaoudi, M.; Vodak, D. T.; Kim, J.; O'Keeffe, M.; Yaghi, O. M. *Science* **2003**, *300*, 1127.
(20) Barthelet, K.; Marrot, J.; Riou, D.; Ferey, G. *Angew. Chem., Int. Ed.* **2002**, *41*, 281.

(21) Ferey, G.; Latroche, M.; Serre, C.; Millange, F.; Loiseau, T.; Percheron-Guegan, A. *Chem. Commun.* **2003**, 2976.
(22) Pan, L.; Liu, H.; Lei, X.; Huang, X.; Olson, D. H.; Turro, N. J.; Li, J. *Angew. Chem., Int. Ed.* **2003**, *42*, 5542.
(23) Seki, K. *Chem. Commun.* **2001**, 1496.
(24) Dybtsev, D. N.; Chun, H.; Yoon, S. H.; Kim, D.; Kim, K. *J. Am. Chem. Soc.* **2004**, *126*, 32.
(25) Soldatov, D. V.; Enright, G. D.; Ripmeester, J. A. *Chem. Mater.* **2002**, *14*, 348.
(26) Moulton, B.; Zaworotko, M. J. *Chem. Rev.* **2001**, *101*, 1629.
(27) Yaghi, O. M.; Li, H.; Davis, C.; Richardson, D.; Groy, T. L. *Acc. Chem. Res.* **1998**, *31*, 474.
(28) Kitaura, R.; Onoyama, G.; Sakamoto, H.; Matsuda, R.; Noro, S.; Kitagawa, S. *Angew. Chem., Int. Ed.* **2004**, *43*, 2684.
(29) Kepert, C. J.; Prior, T. J.; Rosseinsky, M. J. *J. Am. Chem. Soc.* **2000**, *122*, 5158.
(30) Hagrman, D.; Hagrman, P. J.; Zubieta, J. *Angew. Chem., Int. Ed.* **1999**, *38*, 3165.
(31) Kitaura, R.; Kitagawa, S.; Kubota, Y.; Kobayashi, T. C.; Kindo, K.; Mita, Y.; Matsuo, A.; Kobayashi, M.; Chang, H.-C.; Ozawa, T. C.; Suzuki, M.; Sakata, M.; Takata, M. *Science* **2002**, *298*, 2358.
(32) Takamizawa, S.; Nakata, E.; Saito, T. *Angew. Chem., Int. Ed.* **2004**, *43*, 1368.
(33) Halder, G. J.; Kepert, C. J. *J. Am. Chem. Soc.* **2005**, *127*, 7891.
(34) Kondo, M.; Okubo, T.; Asami, A.; Noro, S.; Yoshitomi, T.; Kitagawa, S.; Ishii, T.; Matsuzaka, H.; Seki, K. *Angew. Chem., Int. Ed.* **1999**, *38*, 140.
(35) Boultif, A.; Louer, D. *J. Appl. Crystallogr.* **1991**, *24*, 987.
(36) Katoh, M.; Sakamoto, K.; Kamiyamane, M.; Tomida, T. *Phys. Chem. Chem. Phys.* **2000**, *2*, 4471.
(37) Li, D.; Kaneko, K. *J. Phys. Chem. B* **2000**, *104*, 8940.
(38) Webster, C. E.; Drago, R. D.; Zerner, M. C. *J. Am. Chem. Soc.* **1998**, *120*, 5509.
(39) The molecular volume of CO_2, N_2, O_2, CO_2, and CH_4 was calculated by Gaussian03W software, using B3LYP/6-311G* and "volume" keyword.
(40) Kitaura, R.; Fujimoto, K.; Noro, S.; Kondo, M.; Kitagawa, S. *Angew. Chem., Int. Ed.* **2002**, *41*, 133.
(41) Kitaura, R.; Seki, K.; Akiyama, G.; Kitagawa, S. *Angew. Chem., Int. Ed.* **2003**, 428.
(42) Suh, M. P.; Ko, J. W.; Choi, H. J. *J. Am. Chem. Soc.* **2002**, *124*, 10976.
(43) Kepert, C. J.; Hesek, D.; Beer, P. D.; Rosseinsky, M. J. *Angew. Chem., Int. Ed.* **1998**, *37*, 3158.
(44) Edgar, M.; Mitchell, R.; Slawin, A. M. Z.; Lightfoot, P.; Wright, P. A. *Chem. Eur. J.* **2001**, *7*, 5168.
(45) Carlucci, L.; Cozzi, N.; Ciani, G.; Moret, M.; Proserpio, D. M.; Rizzato, S. *Chem. Commun.* **2002**, 1354.
(46) Uemura, K.; Kitagawa, S.; Kondo, M.; Fukui, K.; Kitaura, R.; Chang, H.-C.; Mizutani, T. *Chem. Eur. J.* **2002**, *8*, 3587.
(47) Dybtsev, D. N.; Chun, H.; Kim, K. *Angew. Chem., Int. Ed.* **2004**, *43*, 5033.
(48) Potential curve was calculated by the addition of Lennard-Jones pair potentials between Ar atoms and framework atoms. Framework atoms, whose r is longer than 20 Å, were neglected.
(49) Vishnyakov, A.; Ravikovitch, P. I.; Neimark, A. V.; Bulow, M.; Wang, Q. M. *Nano Lett.* **2003**, *3*, 713.
(50) Cracknell, R. F. *Phys. Chem. Chem. Phys.* **2001**, *3*, 2091.
(51) Biradha, K.; Hongo, Y.; Fujita, M. *Angew. Chem., Int. Ed.* **2002**, *41*, 3395.
(52) Rowsell, J. L. C.; Spencer, E. C.; Eckert, J.; Howard, J. A. K.; Yaghi, O. M. *Science* **2005**, *309*, 1350.
(53) Rigby, M.; et al. *The Forces between molecules*; Clarendon Press: Oxford, UK, 1986.
(54) Aquilanti, V.; Ascenzi, D.; Bartolomei, M.; Cappelletti, D.; Cavalli, S.; Vitores, M. C.; Pirani, F. *Phys. Rev. Lett.* **1999**, *82*, 69.
(55) Aquilanti, V.; Ascenzi, D.; Bartolomei, M.; Cappelletti, D.; Cavalli, S.; Vitores, M. C.; Pirani, F. *J. Am. Chem. Soc.* **1999**, *121*, 10794.
(56) Long, C. A.; Henderson, G.; Ewing, G. E. *Chem. Phys.* **1973**, *2*, 485.
(57) Couronne, O.; Ellinger, Y. *Chem. Phys. Lett.* **1999**, *306*, 71.
(58) Campargue, A.; Biennier, L.; Kachanov, A.; Jost, R.; Bussery-Honvault, B.; Veyret, V.; Churassy, S.; Bacis, R. *Chem. Phys. Lett.* **1998**, *288*, 734.